Rotation and Kinetic Modifications of the Tokamak Ideal-Wall Pressure Limit

J. E. Menard,[1,*] Z. Wang,[1] Y. Liu,[2] R. E. Bell,[1] S. M. Kaye,[1] J.-K. Park,[1] and K. Tritz[3]
[1]Princeton Plasma Physics Laboratory, Princeton University, Princeton, New Jersey 08543, USA
[2]Culham Centre for Fusion Energy, Culham Science Centre, Abingdon OX14 3DB, United Kingdom
[3]Johns Hopkins University, Baltimore, Maryland 21218, USA

(Received 30 January 2014; revised manuscript received 19 October 2014; published 19 December 2014)

The impact of toroidal rotation, energetic ions, and drift-kinetic effects on the tokamak ideal wall mode stability limit is considered theoretically and compared to experiment for the first time. It is shown that high toroidal rotation can be an important destabilizing mechanism primarily through the angular velocity shear; non-Maxwellian fast ions can also be destabilizing, and drift-kinetic damping can potentially offset these destabilization mechanisms. These results are obtained using the unique parameter regime accessible in the spherical torus NSTX of high toroidal rotation speed relative to the thermal and Alfvén speeds and high kinetic pressure relative to the magnetic pressure. Inclusion of rotation and kinetic effects significantly improves agreement between measured and predicted ideal stability characteristics and may provide new insight into tearing mode triggering.

DOI: 10.1103/PhysRevLett.113.255002 PACS numbers: 52.55.Fa, 52.55.Wq

Magnetic fusion reactors based on the tokamak will require operation at high normalized pressure to efficiently generate high fusion power and to generate sufficient pressure-gradient driven current to confine the plasma in steady state [1,2]. The stability of such configurations is limited primarily by pressure-driven kink instabilities which can grow very rapidly on a near-Alfvénic time scale τ_A of a few hundred μs. Importantly, the placement of a resistive conducting wall near the plasma surface can slow kink growth to time scales on the order of the flux penetration time through the wall $\tau_{\rm wall}$ leading to a much more slowly growing (1–10 ms) resistive wall mode (RWM) [3,4] provided the plasma pressure is below the kink stability limit in the presence of an "ideal" (i.e., superconducting) wall. Both active feedback control [5–9] and plasma rotation and kinetic damping [10–18] have been shown to be capable of stabilizing the RWM to pressure values near the ideal-wall limit (IWL). In contrast, plasma operation above the IWL is generally not possible due to the onset of the ideal wall mode (IWM) which grows and/or propagates too rapidly for practical feedback control. Toroidal plasma rotation Ω_ϕ separates the RWM and IWM branches of the with-wall kink dispersion relation [11], and these modes are distinguished by their characteristic growth rates γ and real frequencies ω. In particular, $\gamma\tau_{\rm wall} \sim 1, \omega\tau_{\rm wall} \sim 1$ for the RWM and $\gamma\tau_A \sim 1\%$–10%, $\omega \sim \Omega_\phi$ for the IWM. At sufficiently high plasma Ω_ϕ, the IWM $\omega\tau_{\rm wall} \gg 1$ and the resistive wall appears superconducting [11].

Rotation and kinetic effects for the IWM are studied for the first time and are found to be important when rotation approaches the ion thermal speed and for high $\beta =$ plasma pressure/magnetic pressure. High Ω_ϕ and β are accessible in neutral beam injection heated spherical tokamaks (STs) [19], and high Ω_ϕ can also be accessed in conventional tokamaks. This Letter describes kinetic stability analysis for several NSTX [20,21] ST plasmas that are RWM stable but unstable to the IWM.

Rotation and kinetic effects are studied using the MARS-K [15,22,23] linear stability code and can be understood from a complex energy functional derived by taking a moment of the perturbed force operator $\vec{F}$ with the mode perpendicular displacement $\vec{\xi}_\perp$ [24]. The resulting dispersion relation is $\delta W + \delta K = 0$ where the perturbed potential energy $\delta W \equiv -\frac{1}{2}\int d^3x \vec{F}\cdot\vec{\xi}^*_\perp$ and the perturbed kinetic energy $\delta K \equiv \frac{1}{2}\int d^3x \rho[\gamma + i(\omega - n\Omega_\phi)]^2|\vec{\xi}_\perp|^2$ where n is the toroidal mode number. The real part of the dispersion relation can be expressed as: $\gamma^2 = \Re e(\delta\hat{W})/\delta K_1$ where $\delta K_1 \equiv -\frac{1}{2}\int d^3x \rho|\vec{\xi}_\perp|^2$. Instability occurs for $\Re e(\delta\hat{W}) < 0$ since δK_1 is real and negative definite. Here, $\delta\hat{W} \equiv \delta W + \delta K_2 = \delta W_f + \delta W_v + \delta W_k + \delta\hat{W}_{\rm rot}$ where $\delta\hat{W}_{\rm rot} = \delta W_{\rm rot} + \delta K_2$ and $\delta K_2 \equiv -\frac{1}{2}\int d^3x \rho(\omega - n\Omega_\phi)^2|\vec{\xi}_\perp|^2 \le 0$ is a mode-plasma differential rotation energy. The nonrotating ideal plasma fluid (δW_f) and vacuum (δW_v) terms are given by standard definitions [25,26], $\delta W_k \equiv \frac{1}{2}\int d^3x(\nabla\cdot\vec{\vec{p}}_k)\cdot\vec{\xi}^*_\perp$ where $\vec{\vec{p}}_k$ is the kinetic pressure tensor, and the rotation potential energy $\delta W_{\rm rot} \equiv \delta W_\Omega + \delta W_{d\Omega} + \delta W_{\rm cf}$. The Coriolis force contributes the first two terms: $\delta W_\Omega = -\int d^3x \rho\Omega_\phi[\gamma + i(\omega - n\Omega_\phi)]\vec{\hat{Z}}\times\vec{\xi}\cdot\vec{\xi}^*_\perp$ and $\delta W_{d\Omega} = \int d^3x R\rho\Omega_\phi\xi^*_{\perp R}\nabla\Omega_\phi\cdot\vec{\xi}$, and the centrifugal force contributes $\delta W_{\rm cf} = \frac{1}{2}\int d^3x R\Omega^2_\phi\vec{\xi}^*_{\perp R}\nabla\cdot\rho\vec{\xi}$. The terms $\delta W_{d\Omega}$ and δK_2 are analogous to Kelvin-Helmholtz drive [27–35], and scalings of the δW terms indicate rotation will significantly impact pressure limits when $\delta\hat{W}_{\rm rot} \sim \delta W_{\nabla p} \Rightarrow v_\phi \sim v_{\text{th-ion}}/\sqrt{q} \Rightarrow \Omega_\phi\tau_A \sim \sqrt{\beta_{\rm thermal}/2q}$.

Kinetic effects [15] enter through mode-particle resonances at small values of the denominator of

$$\delta W_k \propto \frac{n[\omega_{*N} + (\hat{\epsilon}_k - \frac{3}{2})\omega_{*T} + \omega_E] - (\omega - i\gamma)}{n[\langle\omega_D\rangle + \omega_E] + (\alpha n q + l)\omega_b - i\nu_{\text{eff}} - (\omega - i\gamma)},$$

where n is the toroidal mode number, the density (N) nd temperature (T) diamagnetic frequencies ω_* for species index j are $\omega_{*N_j} \equiv (1/eZ_j)(dT_j/d\psi)$ and $\omega_{*T_j} \equiv (T_j/eZ_jN_j)(dN_j/d\psi)$, the normalized particle energy $\hat{\epsilon}_k = E/k_BT$, the $\vec{E}\times\vec{B}$ rotation frequency $\omega_E = d\Phi(\psi)/d\psi$ where $\Phi(\psi)$ is the electrostatic potential on a flux surface with poloidal flux function $\psi = RA_\phi$, $\omega - i\gamma$ is the complex mode frequency, $\langle\omega_D\rangle$ is the bounce-average trapped-particle toroidal precession frequency, α is an integer = 0, 1 for trapped, passing particles, respectively, q is the magnetic safety factor, l is the integer bounce-harmonic number, ω_b is the bounce frequency, and ν_{eff} is the effective collision frequency. Electrons and thermal and fast ions are included in the calculations, and fast ions are modeled as an isotropic slowing-down distribution.

Rotation [36] is included in LRDFIT [37,38] equilibrium reconstructions, assuming the rotation is purely toroidal $[v_\phi = R\Omega_\phi(\psi)]$ and using a modified Grad-Shafranov equation with pressure of the form $p(\psi, R) = \hat{p}(\psi)\exp\{U(\psi)[(R/R_{\text{axis}})^2 - 1]\}$ [39] where $U(\psi) \propto \Omega_\phi^2$. The dominant effect of high rotation is to lower the reconstructed q [40] in the core by $\Delta q \approx -0.1$ to -0.2. MARS-K does not presently include equilibrium rotation and is interfaced to the static equilibrium code CHEASE [41]. The reconstructed $\langle J_\phi/R\rangle(\psi)$ profile is used in CHEASE to approximately conserve $q(\psi)$ and plasma current I_P as pressure is varied. The CHEASE $p(\psi)$ is set to either $\hat{p}$ from the reconstruction or to the measured thermal $\hat{p}$ plus fast-ion pressure $p_{\text{fast}}(\psi)$ from TRANSP [42,43].

The early flat-top phase of NSTX discharges was often unstable to low-frequency $n = 1$ modes with $f =$ 15–30 kHz $\sim f_\phi = \Omega_\phi/2\pi$ that occur at β values far below the calculated static plasma ideal-wall β limit. An important uncertainty in this analysis is fast-ion redistribution or loss [44–46] caused by higher-frequency Alfvénic instabilities. For the first plasma studied, there is good agreement between reconstructed (measured) and TRANSP-calculated stored energy (neutron rate) prior to mode onset. However, Fig. 1(a) shows that thermal + fast-ion β without fast-ion redistribution (blue) is significantly more peaked than the reconstructed total (black), and that fast-ion density profile broadening (red) conserving fast-ion number and stored energy can bring the total β profile into agreement with reconstruction. Figure 1(b) shows the core $q \approx 2$ at mode onset, the deuterium thermal Mach number $M_{s-D} \equiv \bar{R}\Omega_\phi/v_{\text{th}-D}$ has a maximum value of 0.8 which should contribute to mode destabilization, and $M_{s-D} \approx 6 \times \omega_E\tau_A$. The normalized minor radius $= \psi_n^{0.5}$, $\psi_n \equiv (\psi - \psi_{\text{axis}})/(\psi_{\text{edge}} - \psi_{\text{axis}})$, $\bar{R}(\psi_n) \equiv \{\text{Max}[R(\psi_n,\theta)] + \text{Min}[R(\psi_n,\theta)]\}/2$, $R_0 = \bar{R}(1)$, $\tau_A \equiv R_0/v_A$,

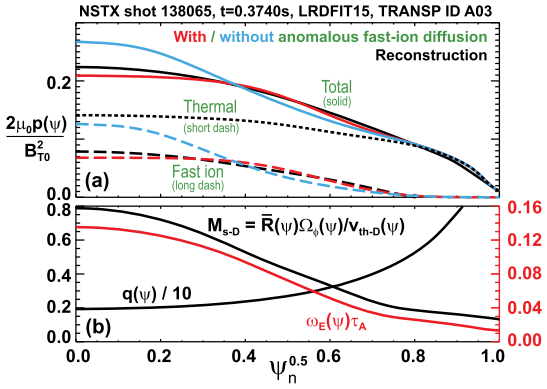

FIG. 1 (color online). Radial profiles of (a) total, thermal, and fast-ion β, and (b) safety factor q and normalized Ω_ϕ and ω_E frequencies.

$v_A \equiv B_{T0}/\sqrt{\mu_0\rho(0)}$, B_{T0} is the vacuum toroidal field at R_0, and $\rho(\psi_n)$ is the plasma mass density profile.

Figure 2(a) shows the amplitude evolution of the $n = 1$ mode which becomes unstable near $t = 0.376$ s with effective mode growth rate $\gamma_{\text{eff}} \approx 1$ ms. Using redistributed fast-ion density profiles consistent with the reconstructed total β as shown in Fig. 1(a), Fig. 2(b) shows the experimental β_N evolution and MARS-K marginal β_N values assuming plasma resistivity $\eta = 0$. These MARS-K IWM calculations benefit from recent extensive code benchmarking for the RWM [47]. Here, β_N [48–50] $\equiv \beta_T a B_{T0}/I_P[\%mT/MA]$, $\beta_T \equiv 2\mu_0\langle p\rangle/B_{T0}^2$, $\langle p\rangle$ is volume-average pressure, and a is the plasma minor radius. Figure 2(b) shows that fluid marginal with-wall β_N limits at low rotation (solid green) are all more than twice the experimental marginal $\beta_N \approx 3.5$. For these calculations,

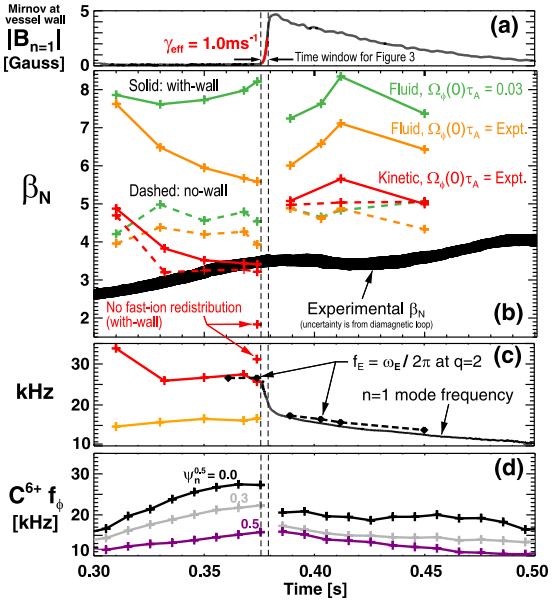

FIG. 2 (color online). Time evolution of: (a) mode amplitude, (b) β_N values, (c) mode frequency, and (d) plasma rotation frequency.

the experimental Ω_ϕ and ω_E profiles are scaled linearly by the same factor such that $\Omega_\phi(0)\tau_A = 0.03$. The marginal with-wall β_N values using the experimental Ω_ϕ (solid orange) decrease from 8.3 to 5.5 at mode onset consistent with increasing destabilization from the increasing f_ϕ shown in Fig. 2(d). Wall stabilization is important at both low and higher Ω_ϕ as evident from the $\Delta\beta_N = 1.5$ to 3 difference between the solid and dashed green and orange curves. As shown by the solid red curves in Fig. 2(b), only full kinetic MARS-K calculations including wall stabilization, experimental Ω_ϕ, and non-Maxwellian fast ions have marginal β_N values consistent with experimental mode onset time and marginal β_N. As indicated by the two red plus symbols with no fast-ion redistribution, the predicted marginal $\beta_N \approx 1.8$ is much lower and the predicted ω higher than experiment, highlighting the importance of fast-ion profile broadening.

Importantly, by 15 ms after mode onset, all computed stability limits are well above the experimental β_N value, but the mode persists for another 120 ms. This suggests the slowly decaying mode in the experiment is a tearing mode possibly triggered [51–55] by proximity to the kinetic IWM limit. Figure 2(c) shows that the kinetic predicted f is near the experimental $f \approx 26$ kHz at mode onset and that the fluid f (orange) is well below this frequency. This implies that fast ions increase the mode f toward f_E at the $q = 2$ surface which may facilitate seeding [56–61] of a $m/n = 2/1$ tearing mode. Figures 2(c) and 2(d) show that the mode f drops by ≈10 kHz within 10 ms after mode onset and $f \approx f_E$ at the $q = 2$ surface thereafter.

To assess whether the observed mode is ideal or resistive at mode onset, the method of Callen [62] is used. Figure 3(a) shows the computed $\hat{\gamma}_{\rm MHD}$ for the kinetic MARS-K analysis at $t = 0.374$ s from Fig. 2. Figure 3(b) shows the experimental $\beta_N(t)$ (black) and the linear fit (green) used to determine γ_h. The predicted marginal $\beta_N = 3.41$ agrees with the experimental marginal $\beta_N = 3.48$ to within the uncertainty of the diamagnetic flux measurement used to constrain β [see Fig. 2(b)]. Using an amplitude smoothing width ≈0.5 ms such that a time-evolving fit to the Callen model $\xi = \xi_0 \exp[(\gamma_{\rm eff} t)^{(1+\alpha)}]$ results in a nearly constant α immediately after mode onset, Fig. 3(c) shows that $1 + \alpha \approx 1.5$ (blue) for the first 0.5 ms of mode growth consistent with ideal instability. This figure also shows the predicted ideal growth-rate evolution $\hat{\gamma}_{\rm MHD}(\gamma_h t)^{1/2}$ (green) is consistent with the fitted $\gamma_{\rm eff}(t)$ (red) for the first 0.5 ms of mode growth.

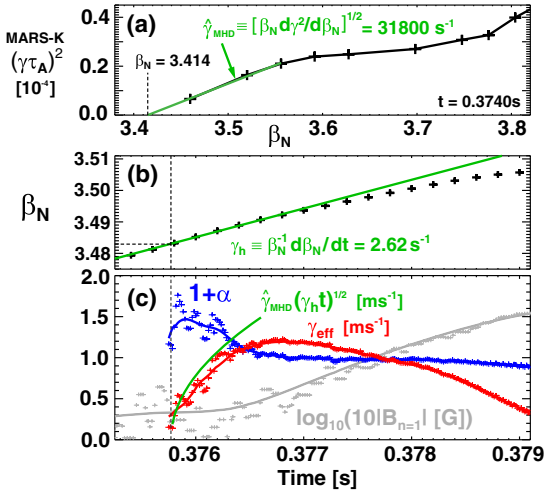

FIG. 3 (color online). (a) MARS-K γ vs β_N, (b) experimental β_N(t), and (c) comparison of measured and predicted effective γ.

Soft x-ray (SXR) data can also be used to check consistency with an ideal eigenfunction. Assuming SXR emission $\epsilon(\psi,\theta,\phi) = \epsilon_0(\psi) + \delta\epsilon(\psi,\theta,\phi)$ and $\delta\epsilon \propto \vec{\xi}\cdot\nabla\epsilon_0$, Fig. 4(a) shows the perpendicular displacement profile from MARS-K and Figs. 4(b)–4(e) show the simultaneous best fit to the 4(b) total emission, 4(c) line-integrated fluctuation amplitude profile, and 4(d) and 4(e) mode phase. The free parameters in the fit are the $\epsilon_0(\psi)$ profile (red) and the MARS-K mode amplitude and phase. As is evident from the figure, the predicted mode eigenfunction peaks between $\psi_n^{0.5} = 0.5$ and 0.8 consistent with the SXR data, and a smoothly increasing $\epsilon_0(\psi)$ profile (from core to edge) can reproduce the mean and fluctuating emission features using the kinetic eigenfunction from MARS-K. SXR fits during the mode decay phase show poor agreement with MARS-K but good agreement with a perturbed-helical-flux island model [39] of a 2/1 tearing mode. Overall, the agreement between the measured and predicted marginal

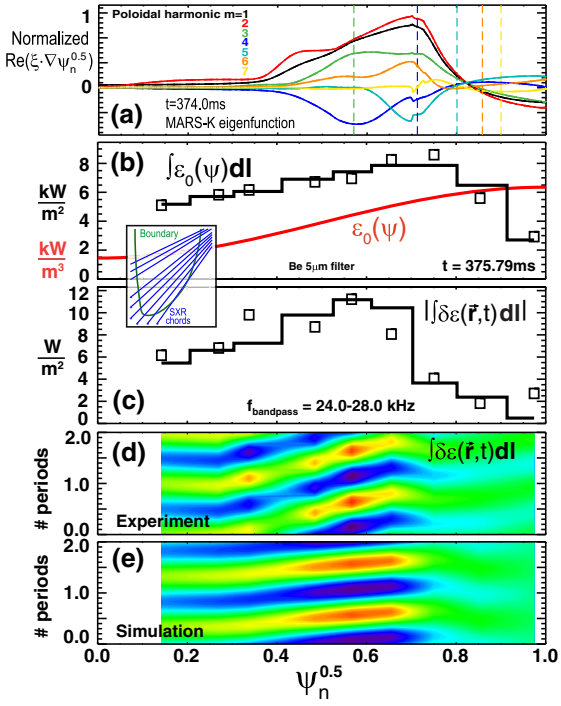

FIG. 4 (color online). (a) MARS-K mode displacement, (b) equilibrium, and (c) fluctuating line-integrated SXR emission from simulation/fit (black lines) and measurement (squares), (d) measured and (e) simulated line-integrated SXR fluctuation signal versus $\psi_n^{0.5}$ and time spanning two mode oscillation periods.

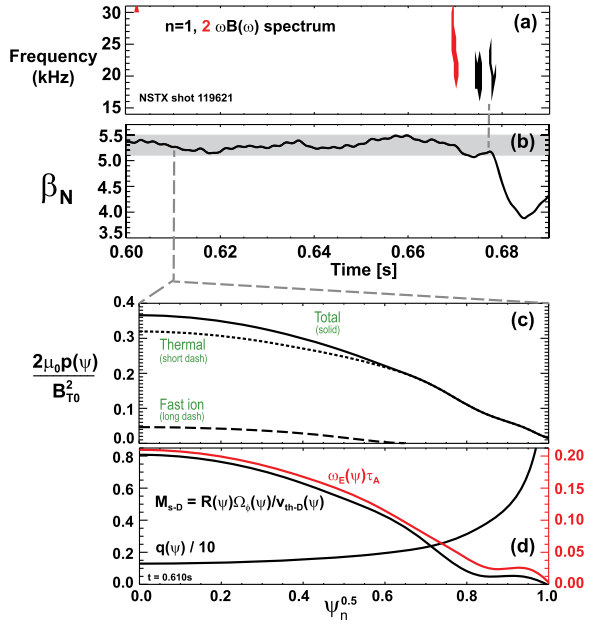

FIG. 5 (color online). Time evolution of: (a) mode frequency, and (b) β_N, radial profiles of: (c) β, (d) q and normalized Ω_ϕ, ω_E.

β_N, ω, γ, and $\vec{\xi}\cdot\nabla\psi_n^{0.5}$ strongly indicate the presence of a kink mode with a β_N limit reduced by rotation and fast ions that initiates an $m/n = 2/1$ tearing mode that subsequently decays after kink drive has been reduced.

The large reduction in marginal β_N from Ω_ϕ and fast ions and resultant triggering of tearing modes is not a universal result. Figure 5 plots the evolution and profiles of a higher $\beta_N = 5.1$–5.5 state typical of the later phases of high-performance NSTX H-mode plasmas in which the minimum q evolves downward to $q_{\min} = 1.2$–1.5. The reconstruction methodology for this shot is the same as for the previous case. It is again found that the TRANSP $\beta_{\text{fast}}(\psi)$ computed without redistribution is significantly more peaked than the reconstructed $\beta_{\text{fast}} =$ reconstructed $\beta_{\text{total}} - \beta_{\text{thermal}}$, and the reconstructed β_{fast} is used in the stability analysis. Figures 5(a) and 5(b) show the onset of a fast-growing $n = 1$ mode which leads to a 25% drop in β_N. Figures 5(c) and 5(d) show β, q, and rotation profiles. $M_{s-D}(\psi_n = 0)$ is again ≈ 0.8 which should contribute to mode destabilization, and $M_{s-D} \approx 4 \times \omega_E \tau_A$.

Figure 6(a) shows that experimental Ω_ϕ again reduces the predicted β_N limit—in this case, from 5.6 (black) to 4.2 (red). However, for this plasma, the inclusion of full kinetic effects substantially restabilizes the rotation-destabilized IWM as indicated by the three γ curves (green, blue, orange) for the varied fast-ion pressure profiles shown in the figure inset. The figure shows variations in fast-ion pressure peaking (consistent with reconstructed p_{total}) lead to only small variations in the marginal $\beta_N = 5.3$–5.5, and that the kinetic marginal β_N is more consistent with the experimental marginal β_N range than the fluid IWM prediction. Figure 6(b) shows that inclusion of kinetic effects results in predicted mode f more consistent with experiment than the fluid treatment, and that the most peaked fast-ion profile

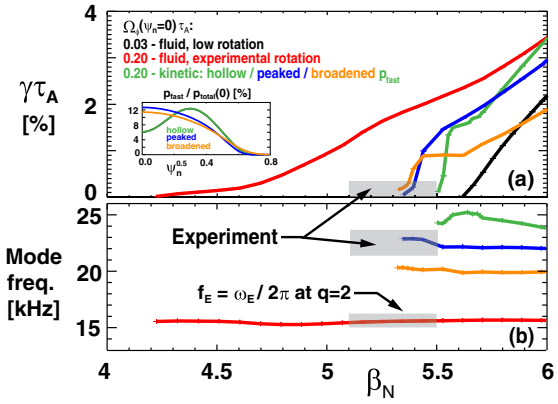

FIG. 6 (color online). (a) Fluid and kinetic IWM γ vs β_N and Ω_ϕ, and (b) predicted and measured mode frequency vs β_N.

(blue) has a mode f most consistent with experiment. Figure 6(b) also shows that the measured/predicted mode $f = 22$–24 kHz is significantly higher than f_E at the $q = 2$ surface (15–16 kHz) which may reduce the drive for tearing mode triggering despite exceeding the IWM β limit.

Figure 7 summarizes the instability drives for both shots near marginal stability and shows the fast-ion δW_{k-f} dominates δW_k and thermal species contribute less. Analysis not shown here finds, for both cases, that δW_{k-f} is dominated by the nonadiabatic part of $\delta W_{k\perp}$ through the precession resonance [63] $\omega \approx \langle\omega_D\rangle + \omega_E$ between $\psi_n^{0.5} = 0.45$ and 0.75, δW_{k-e} is also dominated by the precession resonance, and δW_{k-i} has contributions from precession, bounce, and passing resonances. Figure 7 shows shot 119 621 has a smaller δW_{k-f} fraction consistent with a lower fast-ion β fraction evident from comparing Figs. 5(c) and 1(a). The destabilizing δW_{cur} from the equilibrium $J_\parallel$ is comparable for both shots and is also comparable in magnitude to $\delta\hat{W}_{\text{rot}}$. Shot 138 065 has a more negative $\delta\hat{W}_{\text{rot}}$ than 119 621 consistent with a larger decrease in marginal β_N from rotation, and the rotation-shear-related δK_2 and δW_Ω terms are dominant.

In conclusion, MARS-K linear kinetic stability calculations show that including rotation, slowing down fast ions, and drift-kinetic effects can substantially improve agreement between predicted and measured IWM stability characteristics in rapidly rotating high-β plasmas. Future work will broaden the equilibrium conditions studied,

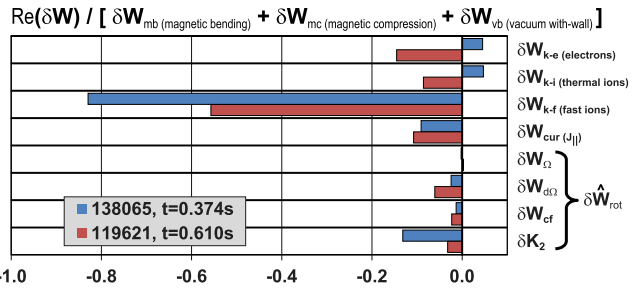

FIG. 7 (color online). Kinetic, $J_\parallel$, and rotation $\text{Re}(\delta\hat{W})$ terms normalized by the sum of positive-definite (i.e., stabilizing) fluid terms.

assess the impact of anisotropic fast ions, and further study tearing mode triggering by the IWM.

This material is based upon work supported by the U.S. Department of Energy, Office of Science, Office of Fusion Energy Sciences under Contract No. DE-AC02-76CH03037 and by the RCUK Energy Programme under Grant No. EP/I501045 and the European Communities under the contract of Association between EURATOM and CCFE. This work was inspired in part by the Max-Planck/Princeton Center for Plasma Physics.

*jmenard@pppl.gov

[1] F. Najmabadi, Fusion Eng. Des. **65**, 143 (2003).
[2] F. Najmabadi *et al.*, Fusion Eng. Des. **80**, 3 (2006).
[3] S. Haney and J. Freidberg, Phys. Fluids B **1**, 1637 (1989).
[4] E. Strait, T. Taylor, A. Turnbull, J. Ferron, L. Lao, B. Rice, O. Sauter, S. Thompson, and D. Wróblewski, Phys. Rev. Lett. **74**, 2483 (1995).
[5] Y. Q. Liu and A. Bondeson, Phys. Rev. Lett. **84**, 907 (2000).
[6] J. Bialek, A. H. Boozer, M. E. Mauel, and G. A. Navratil, Phys. Plasmas **8**, 2170 (2001).
[7] A. Bondeson, Y. Liu, D. Gregoratto, Y. Gribov, and V. D. Pustovitov, Nucl. Fusion **42**, 768 (2002).
[8] S. Sabbagh, R. Bell, J. Menard, D. Gates, A. Sontag, J. Bialek, B. LeBlanc, F. Levinton, K. Tritz, and H. Yuh, Phys. Rev. Lett. **97**, 045004 (2006).
[9] S. Sabbagh *et al.*, Nucl. Fusion **50**, 025020 (2010).
[10] A. Bondeson and D. J. Ward, Phys. Rev. Lett. **72**, 2709 (1994).
[11] M. S. Chu, J. M. Greene, T. H. Jensen, R. L. Miller, A. Bondeson, R. W. Johnson, and M. E. Mauel, Phys. Plasmas **2**, 2236 (1995).
[12] A. Bondeson and M. S. Chu, Phys. Plasmas **3**, 3013 (1996).
[13] A. Garofalo *et al.*, Phys. Rev. Lett. **82**, 3811 (1999).
[14] A. Garofalo, E. Strait, L. Johnson, R. La Haye, E. Lazarus, G. Navratil, M. Okabayashi, J. Scoville, T. Taylor, and A. Turnbull, Phys. Rev. Lett. **89**, 235001 (2002).
[15] Y. Liu, M. S. Chu, I. T. Chapman, and T. C. Hender, Phys. Plasmas **15**, 112503 (2008).
[16] J. W. Berkery, S. A. Sabbagh, R. Betti, B. Hu, R. E. Bell, S. P. Gerhardt, J. Manickam, and K. Tritz, Phys. Rev. Lett. **104**, 035003 (2010).
[17] J. Menard *et al.*, Nucl. Fusion **50**, 045008 (2010).
[18] J. W. Berkery, S. A. Sabbagh, H. Reimerdes, R. Betti, B. Hu, R. E. Bell, S. P. Gerhardt, J. Manickam, and M. Podestà, Phys. Plasmas **17**, 082504 (2010).
[19] Y. Peng and D. Strickler, Nucl. Fusion **26**, 769 (1986).
[20] S. Kaye *et al.*, Fusion Technol. **36**, 16 (1999).
[21] M. Ono *et al.*, Nucl. Fusion **40**, 557 (2000).
[22] Y. Liu *et al.*, Phys. Plasmas **16**, 056113 (2009).
[23] Y. Liu *et al.*, Plasma Phys. Controlled Fusion **52**, 104002 (2010).
[24] I. B. Bernstein, E. A. Frieman, M. D. Kruskal, and R. M. Kulsrud, Proc. R. Soc. A **244**, 17 (1958).
[25] J. P. Freidberg, *Ideal Magnetohydrodynamics* (Plenum Press, New York, 1987).
[26] Z. R. Wang, S. C. Guo, and Y. Q. Liu, Phys. Plasmas **19**, 072518 (2012).
[27] N. D'Angelo, Phys. Fluids **8**, 1748 (1965).
[28] M. Dobrowolny, Phys. Fluids **15**, 2263 (1972).
[29] P. J. Catto, Phys. Fluids **16**, 1719 (1973).
[30] A. B. Mikhailovskii, J. Plasma Phys. **28**, 1 (1982).
[31] M. S. Chu, Phys. Plasmas **5**, 183 (1998).
[32] A. B. Mikhailovskii and S. E. Sharapov, Plasma Phys. Controlled Fusion **42**, 57 (2000).
[33] I. T. Chapman, N. R. Walkden, J. P. Graves, and C. Wahlberg, Plasma Phys. Controlled Fusion **53**, 125002 (2011).
[34] I. Chapman, S. Brown, R. Kemp, and N. Walkden, Nucl. Fusion **52**, 042005 (2012).
[35] C. Wahlberg, J. P. Graves, and I. T. Chapman, Plasma Phys. Controlled Fusion **55**, 105004 (2013).
[36] R. E. Bell, Rev. Sci. Instrum. **77**, 10E902 (2006).
[37] J. Menard *et al.*, Phys. Rev. Lett. **97**, 095002 (2006).
[38] J. Menard, Homepage for the LRDFIT code, http://nstx-u.pppl.gov/software/lrdfit.
[39] J. Menard *et al.*, Nucl. Fusion **45**, 539 (2005).
[40] F. M. Levinton *et al.*, Phys. Plasmas **14**, 056119 (2007).
[41] H. Lütjens, A. Bondeson, and O. Sauter, Comput. Phys. Commun. **97**, 219 (1996).
[42] R. J. Goldston, D. C. McCune, H. H. Towner, S. L. Davis, R. J. Hawryluk, and G. L. Schmidt, J. Comput. Phys. **43**, 61 (1981).
[43] A. Pankin, G. Bateman, R. Budny, A. Kritz, D. McCune, A. Polevoi, and I. Voitsekhovitch, Comput. Phys. Commun. **164**, 421 (2004).
[44] E. D. Fredrickson *et al.*, Phys. Plasmas **13**, 056109 (2006).
[45] S. Gerhardt *et al.*, Nucl. Fusion **51**, 033004 (2011).
[46] E. D. Fredrickson, N. N. Gorelenkov, M. Podesta, A. Bortolon, S. P. Gerhardt, R. E. Bell, A. Diallo, and B. LeBlanc, Nucl. Fusion **54**, 093007 (2014).
[47] J. W. Berkery, Y. Q. Liu, Z. R. Wang, S. A. Sabbagh, N. C. Logan, J.-K. Park, J. Manickam, and R. Betti, Phys. Plasmas **21**, 052505 (2014).
[48] F. Troyon, R. Gruber, H. Saurenmann, S. Semenzato, and S. Succi, Plasma Phys. Controlled Fusion **26**, 209 (1984).
[49] F. Troyon and R. Gruber, Phys. Lett. A **110A**, 29 (1985).
[50] J. E. Menard *et al.*, Phys. Plasmas **11**, 639 (2004).
[51] D. P. Brennan, E. J. Strait, A. D. Turnbull, M. S. Chu, R. J. La Haye, T. C. Luce, T. S. Taylor, S. Kruger, and A. Pletzer, Phys. Plasmas **9**, 2998 (2002).
[52] D. P. Brennan *et al.*, Phys. Plasmas **10**, 1643 (2003).
[53] D. Brennan, S. Kruger, T. Gianakon, and D. Schnack, Nucl. Fusion **45**, 1178 (2005).
[54] S. Gerhardt *et al.*, Nucl. Fusion **49**, 032003 (2009).
[55] D. Brennan, C. Kim, and R. La Haye, Nucl. Fusion **52**, 033004 (2012).
[56] R. Fitzpatrick, Nucl. Fusion **33**, 1049 (1993).
[57] X. Wang and A. Bhattacharjee, Phys. Plasmas **4**, 748 (1997).
[58] C. C. Hegna, J. D. Callen, and R. J. LaHaye, Phys. Plasmas **6**, 130 (1999).
[59] R. J. Buttery, M. Valovi, C. D. Warrick, H. R. Wilson, COMPASS-D Team, and ECRH Teams, Nucl. Fusion **41**, 985 (2001).
[60] R. J. La Haye, Phys. Plasmas **13**, 055501 (2006).
[61] R. J. La Haye, D. P. Brennan, R. J. Buttery, and S. P. Gerhardt, Phys. Plasmas **17**, 056110 (2010).
[62] J. D. Callen, C. C. Hegna, B. W. Rice, E. J. Strait, and A. D. Turnbull, Phys. Plasmas **6**, 2963 (1999).
[63] Y. Liu, I. T. Chapman, J. P. Graves, G. Z. Hao, Z. R. Wang, J. E. Menard, M. Okabayashi, E. J. Strait, and A. Turnbull, Phys. Plasmas **21**, 056105 (2014).